Int. J. Electrochem. Sci., 12 **(2017)** 2376 – 2388, doi: 10.20964/2017.03.51

International Journal of
ELECTROCHEMICAL
SCIENCE
www.electrochemsci.org

Fabrication and Corrosion Resistance of the Ti-rich Alloyed Layer on the Surface of NiTi Alloys

Hairui Wu[1], *Tianzhe Wang*[2], *Xuan Liu, Naiming Lin*[1], *Xiaoping Liu*[1], *Zhiyong He*[1], *Zhenxia Wang*[1,*]

[1] College of Material Science and Engineering, Taiyuan University of Technology, Taiyuan 030024, P. R. China
[2] North Automatic Control Technology Institute Taiyuan 030024, P. R. China
[*]E-mail: wangzhenxia@tyut.edu.cn

Received: 21 October 2016 / *Accepted:* 15 January 2017 / *Published:* 12 February 2017

In this paper, the Ti-rich alloyed layer was prepared on the surface of NiTi alloys by the plasma surface alloying technique. The surface and cross-section morphology, elemental composition distribution and structural characteristics of the films were assessed by scanning electron microscope (SEM), glow discharge optical emission spectroscopy (GDOES) and X-ray diffraction (XRD) techniques, respectively. The thermodynamic and kinetic corrosion properties of the Ti-rich alloyed layer were investigated under simulated body fluid conditions by using open circuit potential and potentiodynamic polarization tests. Electrochemical impedance spectroscopy (EIS) combined with equivalent circuit modelling was implemented to analyze the frequency response. The results showed that the cross-section microstructure was composed of a 10μm thick loose outer deposition layer and an 8μm thick dense inner diffusion layer, including the phases of Ti_2Ni, TiNi and Ti. The passive current density for the Ti-rich alloyed layer was around 1.1×109 A·cm^{-2} and 40 times lower than that of NiTi substrate. The polarization resistance evaluated from the EIS was found to be increased approximately 10 times from 6.133×105 Ω·cm2 for the uncoated NiTi sample to 7.558×106 Ω·cm2 for the alloyed sample. These evidences illustrate that the Ti-rich alloyed layer possess higher corrosion resistance in SBF solution compared to the NiTi substrate. The Mass Spectrometry test results evidenced that the Ti-rich alloyed layer can significant inhibited the release of Ni ion into the human body system.

Keywords: NiTi alloys; Plasma surface alloying; Ti-rich alloyed layer; corrosion resistance; Adhesion strength

1. INTRODUCTION

Equiatomic nickel titanium shape memory alloys (NiTi SMAs) have different crystal structures and performance under the different temperature. The high-temperature phase is austenite phase with

body centered cubic B2 structure which has high hardness, stiffness and stability under low stress. The low-temperature phase is martensite phase and monoclinic with B19 symmetry. Meanwhile NiTi SMAs have excellent ductility, strength, superelasticity, shape memory effect and high damping characteristics [1]. Due to the desirable and superior properties, NiTi SMAs have attracted interests of researchers to be used for medical applications as load-bearing implant materials, such as stents, compression staple and knee joints [2-5]. However, the high nickel content in biomedical NiTi SMAs should be noticed since Ni ions can trigger anaphylactic and adverse reactions once they are released into the human body system [6-9]. In addition, Corrosion and wear occurring on the surface of the implanted NiTi SMAs would expedite the release of Ni ions due to long-term application in the human body.

In order to enhance the corrosion and wear properties of NiTi SMAs and reduce the release of nickel element, surface modification treatment seems to be a feasible method which can reduce the adverse tissue reactions due to implant corrosion, wear particles and release of toxic ions from the corrosion surface, while the vast majority of satisfying performance of the materials would been retained [10]. For implanted NiTi SMAs, variety of surface treatment techniques have been investigated such as anodic oxidation, thermal oxidation, electrochemical deposition and laser surface melting by many researchers [11-16]. Plasma surface alloying (PSA) is an effective surface modification technique that can produce a dense gradient surface modified layer [17-19]. The virtue of this technology has been confirmed.

Titanium is selected to be the surface alloying elements on account of its non-toxicity feature and good biocompatibility. Moreover, titanium is the contained elements in NiTi SMAs and the linear thermal expansion coefficients of both are also similar. Hence the bonding strength of the coating and matrix is higher [20]. Based on prior studies, the primary objective of the current research is to explore the effects of Ti as an alloying element on the electrochemical behaviors in simulated body's internal environment. The corrosion behaviors of uncoated NiTi were also measured as controls.

2. EXPERIMENTAL METHODS

2.1 Specimen preparation

The Ti-50.8%Ni plate with the size of Φ20mm×1mm was used as the substrate materials. The samples were mechanically polished progressively with 180-2000 grits SiC emery papers, and then polished with 0.5μm diamond polishing agent. Finally, the samples were ultrasonic cleaned with acetone and alcohol successively to remove any surface residue and then dried for use.

Ti-rich alloyed layer was prepared by Plasma surface alloying equipment. The instrument adopted the bi-directional pulsed voltage as its exciting source [21, 22]. The cathode voltage was in the range of -350V to -450V, and the source voltage was inside the range of -600V to -800V. Argon gas was chosen as the shielding gas. The alloying process was performed at a substrate temperature of 900 °C with duration of 3 h under a gas pressure of 40 Pa.

2.2 Phase and microstructure characterization

Microstructure of the surface and cross-section of Ti-rich modified layer was observed by scanning electron microscopy (SEM, MIRA3 TESCAN). Composition profile along the depth of the Ti-rich alloyed layer was analyzed by glow discharge optical emission spectroscopy (GDOES, Spectrum GDA750). The phase constitutions was studied with X-ray diffraction (XRD, Philips X'Pert Pro, Holland) using a Cu Kα radiation.

2.3 Scratch tests

Adhesion of the Ti-rich alloyed layer to substrate was evaluated by a scratch tester (Hui jin HT-3002), equipped with a 200 lm radius Rockwell C-type diamond indenter and an acoustic emission (AE) detector. The friction load was gradually increased from 10 to 180 N. The loading rate was 110 N/min and the scratch speed was 2 mm min-1. The critical load (Lc) represented the alloyed layer adhesion strength where the intensity of the acoustic signals occurs sudden increase. The panorama image of the scratched surface was analyzed by optical microscope (Axiovert25CA).

2.4 Electrochemical corrosion studies and Ni ion concentration tests

The corrosion resistance of the samples was carried out by a PMC2000 electrochemical workstation under simulated body fluid (SBF, composition given in Table 1) conditions at 37℃. The potentiodynamic polarization curves and electrochemical impedance spectroscopy (EIS) of the alloyed layer sample and substrate surfaces were conducted to study the corrosion resistance property. A saturated calomel electrode (SCE), a platinum foil and the sample were used as the reference electrode, the counter electrode and the working electrode, respectively. The sweep rate of potentiodynamic polarization curves were 20 $mV \cdot min^{-1}$. The electrochemical impedance spectroscopy (EIS) measurements were expressed with respect to the open circuit potential (OCP) with a small amplitude signal of 10 mV in the frequency range from 100 kHz to 0.01Hz. The solution with a volume of 1ml was collected and stored in polypropylene bottles for further analysis after the corrosion measurements. Mass Spectrometry (ICP-MS7500CE) was employed to analyze the Ni ion release content of the alloyed layer and NiTi substrate.

Table 1. The composition of simulated body fluid

Component	Concentration (g/l)
NaCl	8.035
NaHCO3	0.355
KCl	0.225
K2HPO4·3H2O	0.231
MgCl2·6H2O	0.311
CaCl2	0.292
NaSO4	0.072
Tris	6.118

3. RESULTS AND DISCUSSION

3.1 Surface characterization

The surface morphology and cross-section microstructure of the Ti-rich alloyed layer are shown in Fig. 1 and Fig. 2, respectively. The surface morphology of the Ti-rich alloyed layer exhibited a smooth outer surface and dense appearance. The Ti-rich alloyed layer was formed uniformly on the surface. The cross-section microstructure showed a double structure which was constructed of a 10μm thick loose outer deposition layer and an 8μm thick dense inner diffusion layer. It can be found some pores in the deposition layer. The interface between diffusion layer and substrate exhibited good adhesion due to the metallurgical bonding, which did not exist porosity and crack.

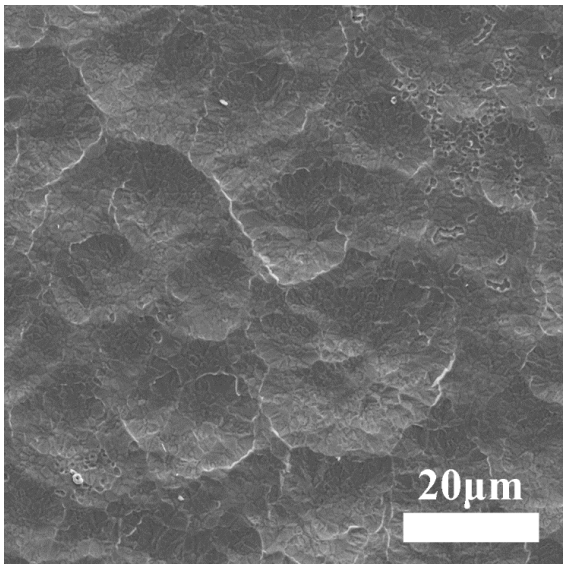

Figure 1. The surface morphology of the Ti-rich alloyed layer

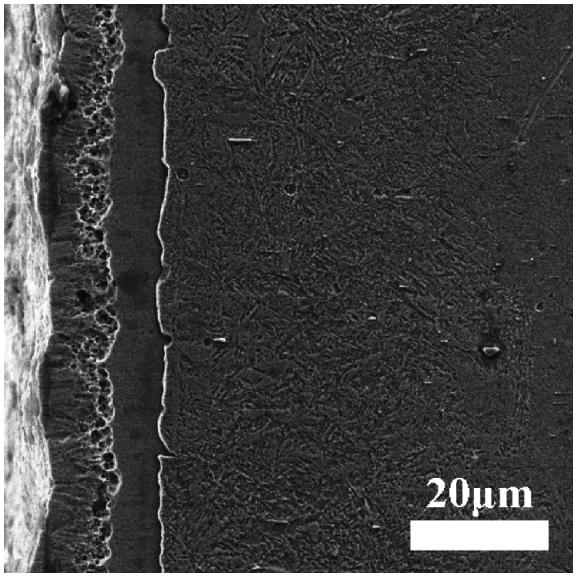

Figure 2. The cross-section microstructure of the Ti-rich alloyed layer

Fig. 3 shows the composition profile along the depth of the Ti-rich alloyed layer. The result presented the concentration of Ni element and Ti element stepwise increased and decreased from the surface to the interior, respectively. The Ni content on the surface reduced from 50.8% to 30%. It indicated that the Ti-rich alloyed layer can successfully decrease the amount of nickel content on the surface of NiTi. The thickness of the Ti-rich alloyed layer was approximately 18μm, which was consistent with the results of Fig. 2.

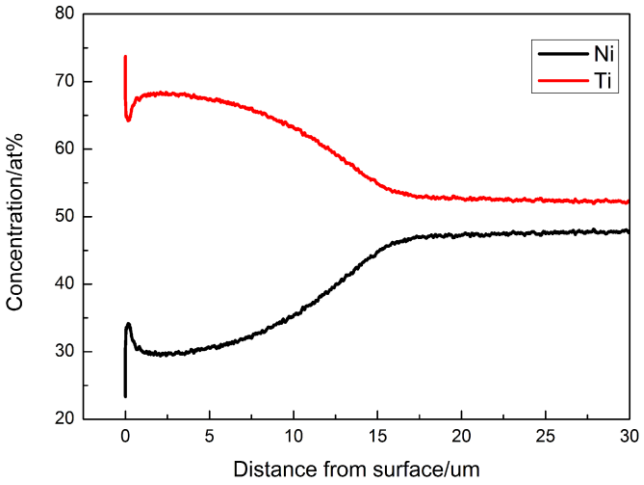

Figure 3. The glow discharge optical emission spectroscopy (GDOES) of the Ti-rich alloyed layer

Fig. 4 shows the XRD spectrum of the Ti-rich alloyed layer. It was confirmed that the Ti-rich alloyed layer was a compound layer and the phase constituents of the Ti-rich alloyed layer consisted of mainly Ti_2Ni, elemental Ti and TiNi. Intermetallic compound Ti_2Ni was formed. Ti_2Ni with face-center-cubic (FCC) crystal structure has high intensity and hardness. In addition, the Ti_2Ni formation was coupled with 30 percent of Ni content on the surface.

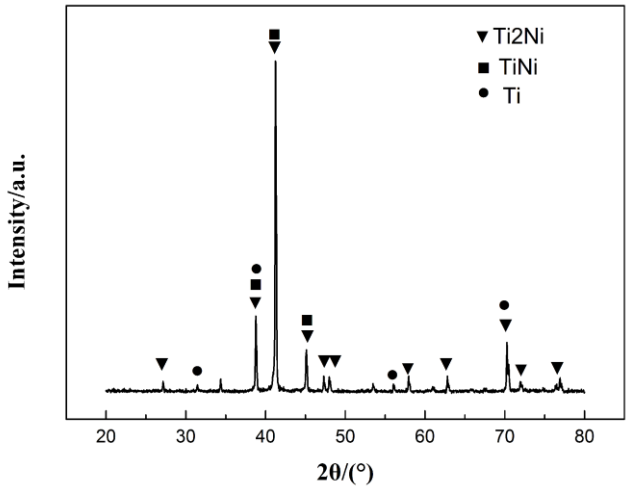

Figure 4. The XRD spectrum of the Ti-rich alloyed layer

3.2 Adhesion strength

The scratch profiles and the image of the scratched surface of the Ti-rich alloyed layers are shown in Fig. 5. Acoustic emission spectra and frictional force vs normal force curves are shown in Fig. 5a. Adhesion strength is evaluated by the critical load. The Ti-rich alloyed layer will appear micro crack, stripping and plastic collapsing with the increase of the normal load. When the intensity of acoustic emission signal becomes stronger abruptly and the frictional force curve appears knee point [23], it indicated the critical stripping of the Ti-rich alloyed layer from the substrate. However, it could also cause by the bulky grain of the Ti-rich alloyed layer. As shown in Fig.5a, the acoustic emission signal increased abruptly at the normal load around 42 N, while frictional force vs normal force curves presented a straight line up. Combined with the image of the scratched surface, as shown in Fig. 5b, analysis that it caused by microcrack and bulky grain principally at 42 N of the normal load. In contrast, the signal peak have the highest acoustic emission intensity and the frictional force appear knee point at the normal load around 72 N. Therefore, the critical load of the Ti-rich alloyed layer was 72 N. The result demonstrated that the Ti-rich alloyed layer possessed a good adhesive strength with NiTi substrate.

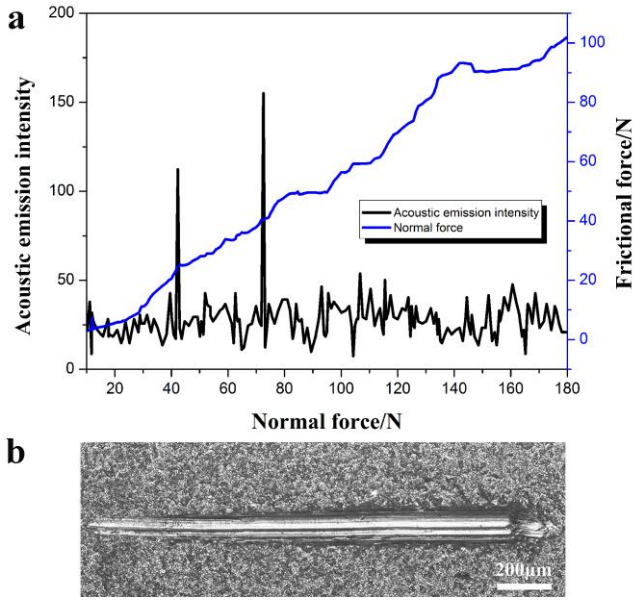

Figure 5. The scratch profiles and panorama image of the scratched surface of the Ti-rich alloyed layers

3.3 Electrochemical corrosion studies

Fig. 6 shows the evolution of the open circuit potential (E_{OCP}) for the Ti-rich alloyed layer and NiTi substrate in SBF solution. The E_{OCP} can indicate the thermodynamic tendency of material participate in the electrochemical corrosion reactions in the corrosive medium [24-26]. The higher E_{OCP} indicates a lower tendency to go through corrosion reactions [27]. It can be see that the shape and

characterized of two E_{OCP} vs. time curves were similar. The E_{OCP} value of the Ti-rich alloyed layer and NiTi substrate were kept around 27 mV and -260 mV, respectively. The positive value and stable state behavior of E_{OCP} for the Ti-rich alloyed layer can be attributed to the Ti_2Ni phase formed. The observed shift in E_{OCP} to positive values for the Ti-rich alloyed layer may indicate the driving force decrease the corrosion process and the Ti-rich alloyed layer can improve thermo dynamically stable in the SBF corrosive medium [28][29]. Further, the results suggested that the Ti-rich alloyed layer produced by the PAS process on the surface of NiTi has improved its corrosion behavior in comparison to NiTi alloy substrate immersed in SBF solution.

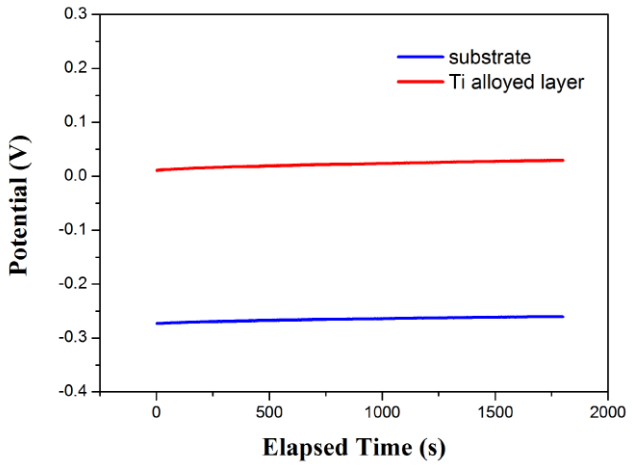

Figure 6. The open circuit potential (E_{OCP}) for the Ti-rich alloyed layer and NiTi substrate

The potentiodynamic polarization curves of the alloyed layer and NiTi substrate in SBF solution are shown in Fig. 7, and the corresponding electrochemical parameters derived from the potentiodynamic polarization curves using Tafel extrapolation are summarized in Table 2. The anodic polarization curves were divided into three regions by three characteristic electric potential (current potential E_{corr}, passive potential E_p, transpassive potential E_{tp}), namely active region, passive region and transpassive region. As shown in Fig. 7, in the initial period of their anodic polarization curves, the active region, the current density increased rapidly with the increase of the anodic potentials. The curves revealed a passive region when anodic potential increase to E_p. It is well know that the smaller E_p and passive current density (I_p) values, the easier the passive film formed in this region. It shows that the passive current density (I_p) of the alloyed layer was around 12.5×10^{-9} $A\cdot cm^{-2}$, which was two orders of magnitude lower than that of NiTi substrate, and the passive potential of the alloyed layer and NiTi substrate were around 75 mV and -190 mV, respectively. The passive potential of the alloyed layer moved in the smaller anodic direction, suggesting that the passive film was more easily formed on the surface of the alloyed layer. However, the passive region of NiTi substrate was significantly larger than that for the alloyed layer. This phenomena mostly because the surface of the alloyed layer exist some loose pores and microcrack, as shown in Fig. 2, lead to lower stability compared with NiTi substrate. In addition, the anodic and cathodic Tafel slopes (b_a and b_c) reported in Table 2. Obviously,

the anodic Tafel slope b_a of the Ti-rich alloyed layer sample was higher than that of the NiTi substrate indicating that the Ti-rich alloyed layer can effectively inhibit the anodic corrosion reaction. Moreover, the polarization resistance (Rp) were calculated by Stern-Geary equation [30] and the results are reported in Table 2.

$$R_p = \frac{b_a \cdot b_c}{2.303 i_{corr}(b_a + b_c)}$$

The polarization resistance of the Ti-rich alloyed layer was $3.8\times10^6\ \Omega\cdot cm^2$, which was significantly higher than that of the NiTi substrate. It is further demonstrated that the alloyed layer can resist the attack of corrosive ions through the alloyed layer and move to the metal/film interface [28, 31, 32]. Further, the corrosion tests results showed a significant shift of the whole polarization curve for the alloyed layer sample towards the region of higher corrosion potential and lower corrosion current density, especially the corrosion current density for the alloyed layer sample was almost 40 times lower than that of NiTi substrate, and therefore it restrained electrochemical reaction over its surface[33, 34]. In conclusion, the corrosion resistance performance of NiTi alloys was significantly improve by preparing Ti-rich alloyed layer on its surface using plasma surface alloying technique.

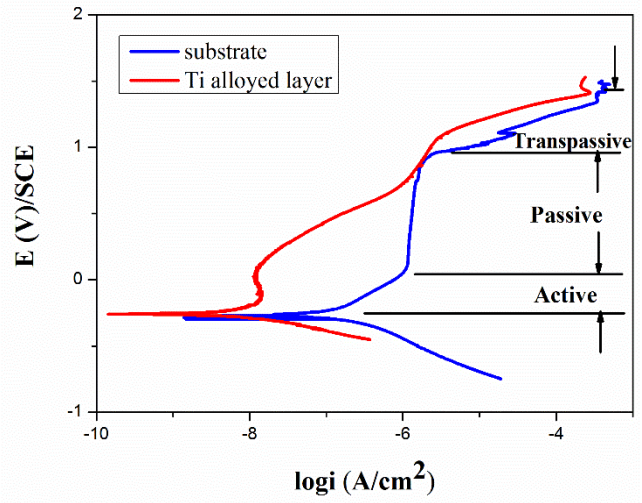

Figure 7. The potentiodynamic polarization curves of the alloyed layer and NiTi substrate

Table 2. Electrochemical parameters extracted from potentiodynamic polarization curves

Sample	NiTi	Alloyed layer
E_{corr} (mV)	-270	-256
I_{corr} ($A\cdot cm^{-2}$)	2.76×10^{-7}	1.1×10^{-9}
E_p (mV)	75	-190
E_b (mV)	900	100
I_p ($A\cdot cm^{-2}$)	1.2×10^{-6}	12.5×10^{-9}
b_a(mV)	252	572
b_c (mV)	175	139
R_p ($\Omega\cdot cm^2$)	1.4×10^5	3.8×10^6

Fig. 8 shows the electrochemical impedance spectroscopy for the alloyed layer and NiTi substrate at respective open circuit potentials in SBF solution, used to analyze the mechanism of corrosion and passivation phenomena[35, 36]. As Fig. 8a shows, the shape of the Nyquist plots for the alloyed layer and NiTi substrate shows capacitive semicircle in the entire frequency range. It can be see that the semicircles of the NiTi substrate are more depressed than those for the Ti-rich alloyed layer, reflecting that formation of the passive film more easily [37]. The Bode plot obtained from the alloyed layer sample and the NiTi substrate are shown in Fig. 8b. The abscissa is plotted by the base 10 logarithm of the frequency (log f) and the ordinate are plotted by the base 10 logarithm of the impedance magnitude (log |Z|) and the negative of the phase angle (-θ). It can be found that the impedance magnitude close to a constant with the phase angle dropping in high frequency range, suggesting that the impedance is controlled by solution resistance in this frequency range. The alloyed layer sample exhibited much higher impedance magnitude in the high frequency domain compared the NiTi substrate sample, considering the fact that the high frequency impedance usually reflects the resistance of the coating. However, in the low frequency range, the NiTi substrate sample presented a higher impedance magnitude. Besides, the phase angle showed the slightly downward tendency in the low frequency region and it indicated that polarization resistance was main contributions to the impedance. However, phase angles approaching 90° in medium to low frequencies range indicated the highly capacitive characteristic, testifying that a highly stable passive layer was formed on the sample surface in the SBF electrolyte [10]. Furthermore, the Bode plots of NiTi substrate existed a single time constant, therefore the electrochemical behavior can be described by the polarization resistance (R_p) and a constant phase element (CPE) in parallel, and the equivalent circuit $R_s(Q_pR_p)$ is shown in Fig. 9(a). According to the characteristics of the alloyed layer prepared by PSA, namely, outer deposition layer and inner diffusion layer (seen in Fig. 2), the equivalent circuit $R_s(Q(R(QR)))$ can be built for the alloyed layer sample as shown in Fig. 9(b). CPE1 corresponds to the high frequency characteristics of outer deposition layer and CPE2 corresponds to the low frequency characteristics of inner diffusion layer. R_s corresponds to the resistance of the solution, while R_p and R_c are the resistance of the outer deposition layer and the inner diffusion layer, respectively. The results of the fitting parameters for simulative EIS of the Ti-rich alloyed layer and NiTi substrate are shown in Table 3. Polarization resistance values for the alloyed layer was around $7.558\times10^6\ \Omega\cdot cm^2$ one order of magnitude higher than that of NiTi substrate ($6.133\times10^5\ \Omega\cdot cm^2$), indicating significantly improvement in the corrosion resistance protection of the NiTi substrate [38]. It was found that the resistance value of the outer deposition layer R_c was $3.461\times10^6\ \Omega\cdot cm^2$, which was less than that of the inner diffusion layer. The lower resistance for the outer deposition layer may result in pores and microcrack in the outer deposition layer. Therefore, the polarization resistance value of the inner diffusion layer R_p was played a decisively role to protect the NiTi substrate.

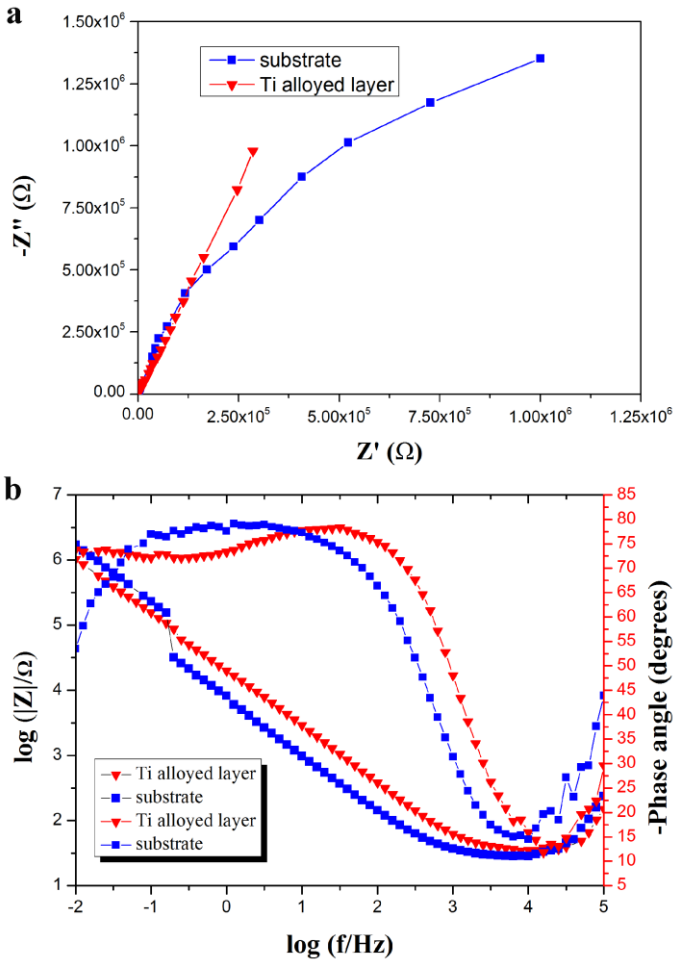

Figure 8. The Nyquist and Bode plots for the alloyed layer and NiTi substrate

Table 3. Electrochemical parameters derived from impedance fitting

Sample	R_s ($\Omega \cdot cm^2$)	CPE1-T	CPE1-P	R_p ($\Omega \cdot cm^2$)	CPE2-T	CPE2-P	R_c ($\Omega \cdot cm^2$)
Substrate	25.6	3.656×10^{-5}	1.083	6.133×10^{5}	-	-	-
Alloyed layer	59.6	1.110×10^{-5}	0.871	7.558×10^{6}	1.107×10^{-5}	0.854	3.461×10^{6}

The Ni ion concentrations in the SBF solution of the Ti-rich alloyed layer and TiNi substrate are shown in Fig. 10. It was clear that the Ni ion concentrations of the Ti-rich alloyed layer sample was significant lower than that of untreated NiTi substrate and the concentration values were 37 ppb and 13030 ppb, respectively. The results indicated that the Ti-rich alloyed layer have successfully inhibited the release of Ni ion into the human body system. Plasma surface Ti alloying could be a potential surface modification treatment to be employed to improve the biomedical performance of NiTi alloys.

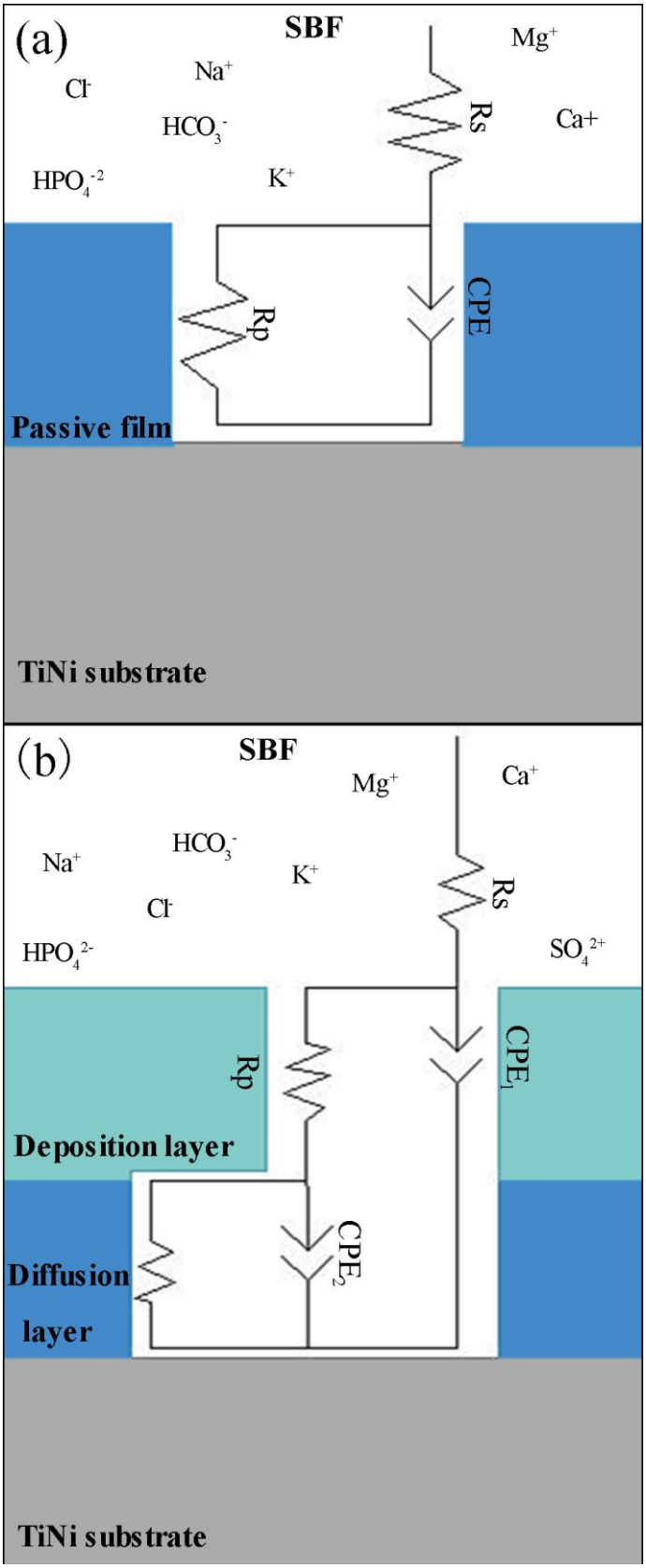

Figure 9. Electrical equivalent circuit (a) for the NiTi substrate and (b) for the alloyed layer sample

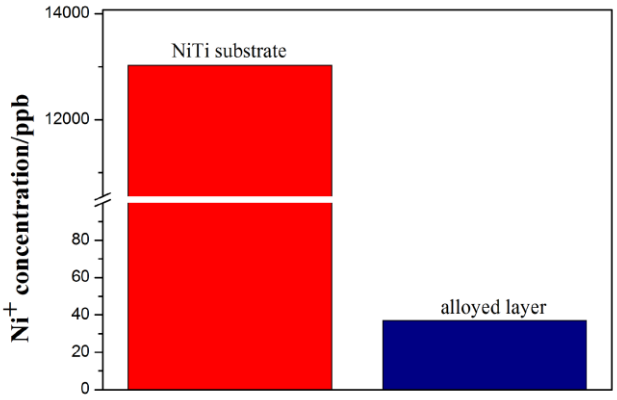

Figure 10. The Ni ion concentrations in the SBF solution of the Ti-rich alloyed layer and TiNi substrate

4. CONCLUSION

The Ti-rich alloyed layer was successfully prepared on the surface of the equiatomic NiTi alloys using plasma surface alloying technique. The following conclusions can be obtained by above detailed experiments and systematic analysis:

1. The Ti-rich alloyed layer was composed of a 10μm thick loose outer deposition layer and an 8μm thick dense inner diffusion layer, and the phase constituents consisted of mainly Ti_2Ni, elemental Ti and TiNi.

2. The Ti-rich alloyed layer possessed a good adhesive strength with NiTi substrate. The critical load of the Ti-rich alloyed layer was 72 N.

3. The open circuit potential of the Ti-rich alloyed layer was towards more noble values which indicated a higher thermodynamic stability compared to that of the untreated substrate. The passive current density for the Ti-rich alloyed layer was around was around 1.1×10^{9} A/cm^2 and 40 times lower than that of NiTi substrate. The polarization resistance evaluated from the EIS was found to be increased approximately 10 times from 6.133×10^{5} Ω·cm^2 for the uncoated sample to 7.558×10^{6} Ω·cm^2 for the alloyed sample. These evidences illustrated that the Ti-rich alloyed layer possessed higher corrosion resistance in SBF solution compared to the NiTi substrate.

4. It is evidenced that the Ti-rich alloyed layer can significant inhibit the release of Ni ion into the human body system.

ACKNOWLEDGMENTS
This research project was supported by the Natural Science Foundation of Shanxi Province, China (2014011015-7), the National Natural Science Foundation of China (51474154,51501125,51471191), and Research Project Supported by Shanxi Scholarship Council of China (2013-048) and the China Postdoctoral Science Foundation (No.2016M591415).

References

1. K.W. Ng, H.C. Man, T.M. Yue, *Appl. Surf. Sci.*, 254 (2008) 6725.

2. L. Tan, *Biomaterials*, 24 (2003) 3931.
3. D. Stoeckel, *Minim Invasive Ther Allied Technol*, 9 (2000) 81.
4. S. Thompson, *Int. Endod. J.*, 33 (2000) 297.
5. K.W. Ng, H.C. Man, T.M. Yue, *Appl. Surf. Sci*., 257 (2011) 3269.
6. K. Matsumoto, N. Tajima, S. Kuwahara, *Nihon Seikeigeka Gakkai zasshi*, 67 (1993) 267.
7. L. El Medawar, P. Rocher, J. Hornez, C, M. Traisnel, J. Breme, H. Hildebrand, *Biomol. Eng*, 19 (2002) 153.
8. S.D. Plant, D.M. Grant, L. Leach, *Biomaterials*, 26 (2005) 5359.
9. J.L. Xu, F. Liu, F.P. Wang, L.C. Zhao, *Mater. Lett*., 62 (2008) 4112.
10. L. Liu, J. Xu, P. Munroe, J. Xu, Z.H. Xie, *Acta Biomater*, 10 (2014) 1005.
11. F.T. Cheng, P. Shi, H.C. Man, *Scr. Mater.*, 51 (2004) 1041.
12. C. Yang, F. Chen, S. Chen, *Mater. Chem. Phys.*, 100 (2006) 268.
13. M.H. Wong, F.T. Cheng, H.C. Man, *Appl. Surf. Sci*., 253 (2007) 7527.
14. Z.D. Cui, H.C. Man, X.J. Yang, *Surf. Coat. Technol.*, 192 (2005) 347.
15. F.T. Cheng, P. Shi, G.K.H. Pang, M.H. Wong, H.C. Man, *J. Alloys Compd*., 438 (2007) 238.
16. G.S. Firstov, R.G. Vitchev1, H. Kumar, B. Blanpain, J.V. Humbeeck, *Biomaterials*, 23 (2002) 4863.
17. Z. Wang, Z. He, Y. Wang, X. Liu, B. Tang, *Appl. Surf. Sci*., 257 (2011) 10267.
18. Z.X. Wang, Z.Y. He, Y.Q. Wang, X.P. Liu, B. Tang, in: Materials Science Forum, Trans Tech Publ, 2011, pp. 759.
19. Z. He, Z. Wang, W. Wang, A. Fan, Z. Xu, *Surf. Coat. Technol*., 201 (2007) 5705.
20. L.C. Campanelli, L.T. Duarte, P.S.C.P. da Silva, C. Bolfarini, *Mater. Des*., 64 (2014) 393.
21. Z. Xu, X. Liu, P. Zhang, Y. Zhang, G. Zhang, Z. He, *Surf. Coat. Technol*., 201 (2007) 4822.
22. W. Wang, Z. Xu, Z. He, Z. Wang, P. Zhang, *Vacuum*, 81 (2007) 937.
23. H. Zhang, Z. Wang, H. Yang, X. Shan, X. Liu, S. Yu, Z. He, *Journal of Wuhan University of Technology-Mater. Sci*. Ed., 31 (2016) 910.
24. K. Venkateswarlu, N. Rameshbabu, D. Sreekanth, M. Sandhyarani, A. Bose, C, V. Muthupandi, S. Subramanian, *Appl. Surf. Sci*., 258 (2012) 6853.
25. N. Lin, H. Zhang, J. Zou, P. Han, Y. Ma, B. Tang, *Int. J. Electrochem. Sci*, 10 (2015) 356.
26. N. Lin, P. Zhou, H. Zhou, J. Guo, H. Zhang, J. Zou, Y. Ma, P. Han, B. Tang, *Int. J. Electrochem. Sci*, 10 (2015) 2694.
27. M. Karthega, S. Nagarajan, N. Rajendran, *Electrochim. Acta*, 55 (2010) 2201.
28. K. Venkateswarlu, N. Rameshbabu, D. Sreekanth, M. Sandhyarani, A. Bose, C, V. Muthupandi, S. Subramanian, *Electrochim. Acta*, 105 (2013) 468.
29. S. Karimi, T. Nickchi, A. Alfantazi, *Corros. Sci*., 53 (2011) 3262.
30. M. Stern, A.L. Geary, *J. Electrochem. Soc*., 104 (1957) 56.
31. M. Kaseem, Y.G. Ko, *J. Electrochem. Soc*., 163 (2016) C587.
32. M. Curioni, P. Skeldon, G.E. Thompson, *Electrochim. Acta*, 105 (2013) 642.
33. Z. Gao, S. Zhao, Y. Wang, X. Wang, L. Wen, *Int. J. Electrochem. Sci*, 10 (2015) 637.
34. Z. Liu, X. Liu, U. Donatus, G.E. Thompson, P. Skeldon, *Int. J. Electrochem. Sci*, 9 (2014) 3558.
35. K.A. Khalil, E.-S.M. Sherif, A.A. Almajid, *Int. J. Electrochem. Sci*, 6 (2011) 6184.
36. M.A. Alam, E.-S.M. Sherif, S.M. Al-Zahrani, *Int. J. Electrochem. Sci*, 8 (2013) 3121.
37. B. Munirathinam, L. Neelakantan, *J. Electrochem. Soc*., 163 (2016) D336.
38. J.L. Xu, F. Liu, F.P. Wang, D.Z. Yu, L.C. Zhao, *J. Alloys Compd*., 472 (2009) 276.